Compensatory Guaiacyl Lignin Biosynthesis at the Expense of Syringyl Lignin in *4CL1*-Knockout Poplar[1][OPEN]

Chung-Jui Tsai,[a,b,c,d,2,3] Peng Xu,[a,b,4] Liang-Jiao Xue,[a,b,d,5] Hao Hu,[a,b,6] Batbayar Nyamdari,[a] Radnaa Naran,[a] Xiaohong Zhou,[a,7] Geert Goeminne,[e,f,8] Ruili Gao,[g,h] Erica Gjersing,[i,j,9] Joseph Dahlen,[a] Sivakumar Pattathil,[j,k,10] Michael G. Hahn,[c,d,j,k] Mark F. Davis,[d,i,j] John Ralph,[g,h] Wout Boerjan,[e,f] and Scott A. Harding[a,b]

[a]Warnell School of Forestry and Natural Resources, University of Georgia, Athens, Georgia 30602
[b]Department of Genetics, University of Georgia, Athens, Georgia 30602
[c]Department of Plant Biology, University of Georgia, Athens, Georgia 30602
[d]Center for Bioenergy Innovation, Oak Ridge National Laboratory, Oak Ridge, Tennessee 37831
[e]Department of Plant Biotechnology and Bioinformatics, Ghent University, 9052 Ghent, Belgium
[f]Vlaams Instituut voor Biotechnologie, UGent Center for Plant Systems Biology, 9052 Ghent, Belgium
[g]Department of Biochemistry, University of Wisconsin-Madison, Madison, Wisconsin 53706
[h]Great Lakes Bioenergy Research Center, Wisconsin Energy Institute, University of Wisconsin-Madison, Madison, Wisconsin 53726
[i]National Renewable Energy Laboratory, Golden, Colorado 80401
[j]BioEnergy Science Center, Oak Ridge National Laboratory, Oak Ridge, Tennessee 37831
[k]Complex Carbohydrate Research Center, University of Georgia, Athens, Georgia 30602

ORCID IDs: 0000-0002-9282-7704 (C.-J.T.); 0000-0001-8007-9879 (P.X.); 0000-0003-1766-5298 (L.-J.X.); 0000-0003-4986-2034 (H.H.); 0000-0002-0337-2999 (G.G.); 0000-0002-2073-7224 (E.G.); 0000-0003-3870-4137 (S.P.); 0000-0003-2136-5191 (M.G.H.); 0000-0003-4541-9852 (M.F.D.); 0000-0002-6093-4521 (J.R.); 0000-0003-1495-510X (W.B.); 0000-0001-5098-2370 (S.A.H.).

The lignin biosynthetic pathway is highly conserved in angiosperms, yet pathway manipulations give rise to a variety of taxon-specific outcomes. Knockout of lignin-associated *4-coumarate:CoA ligases* (*4CLs*) in herbaceous species mainly reduces guaiacyl (G) lignin and enhances cell wall saccharification. Here we show that CRISPR-knockout of *4CL1* in poplar (*Populus tremula* × *alba*) preferentially reduced syringyl (S) lignin, with negligible effects on biomass recalcitrance. Concordant with reduced S-lignin was downregulation of *ferulate 5-hydroxylases* (*F5Hs*). Lignification was largely sustained by 4CL5, a low-affinity paralog of 4CL1 typically with only minor xylem expression or activity. Levels of caffeate, the preferred substrate of 4CL5, increased in line with significant upregulation of *caffeoyl shikimate esterase1*. Upregulation of *caffeoyl-CoA O-methyltransferase1* and downregulation of *F5Hs* are consistent with preferential funneling of 4CL5 products toward G-lignin biosynthesis at the expense of S-lignin. Thus, transcriptional and metabolic adaptations to *4CL1*-knockout appear to have enabled 4CL5 catalysis at a level sufficient to sustain lignification. Finally, genes involved in sulfur assimilation, the glutathione-ascorbate cycle, and various antioxidant systems were upregulated in the mutants, suggesting cascading responses to perturbed thioesterification in lignin biosynthesis.

The angiosperm lignin biosynthetic pathway has been studied for decades and continues to be a topic of interest thanks to its plasticity (Sederoff et al., 1999; Boerjan et al., 2003; Ralph et al., 2004). A host of factors likely contribute to the plasticity of lignification, including enzyme redundancy and taxon-dependent properties during development or in response to environmental pressures (Weng and Chapple, 2010; Vanholme et al., 2019). 4-Coumarate:CoA ligase (4CL) catalyzes ATP-dependent CoA-thioesterification of various cinnamic acid derivatives (Knobloch and Hahlbrock, 1975) in arguably the most promiscuous step of monolignol biosynthesis. In all sequenced angiosperm genomes, 4CL is encoded by multiple genes belonging to two distinct phylogenetic classes (Ehlting et al., 1999; Saballos et al., 2012; Chen et al., 2014b). Although Class-II 4CLs involved in the biosynthesis of flavonoids and other soluble phenolics exhibit a substrate preference for 4-coumaric acid, many lignin-associated Class-I members show similar in vitro affinities for caffeic acid, 4-coumaric acid, and sometimes ferulic acid (Ehlting et al., 1999; Harding et al., 2002; Lindermayr et al., 2002; Gui et al., 2011; Chen et al., 2013).

The poplar (*Populus trichocarpa* Nisqually-1) genome contains four Class-I *4CL* members as two paralogous pairs derived from Salicoid whole-genome duplication (Supplemental Fig. S1; Tsai et al., 2006). Among them, *4CL1* (Potri.001G036900) is known to be involved in lignin biosynthesis based on molecular and reverse genetic characterization in *Populus tremuloides* and *Populus*

tremula × *alba* INRA 717-1B4 (Hu et al., 1998, 1999; Voelker et al., 2010). The genome duplicate *4CL5* (Potri.003G188500) is the only other *4CL* gene family member expressed in lignifying xylem, but its transcript levels are much lower than those of *4CL1* (Supplemental Fig. S1; Hefer et al., 2015; Swamy et al., 2015; Hu et al., 2016; Xue et al., 2016; Wang et al., 2018). *4CL1* and *4CL5* were proposed to encode 4CL proteins that form heterotetramers in a 3:1 ratio (referred to as Ptr4CL3 and Ptr4CL5 in Chen et al. [2013, 2014a]). The activity of individual isoforms as well as the tetrameric complex is sensitive to inhibition by hydroxycinnamic acids and their shikimate esters (Harding et al., 2002; Chen et al., 2014a; Lin et al., 2015). Such complexity of 4CL catalysis is consistent with multiple cellular strategies for directing hydroxycinnamic acids toward lignin biosynthesis. Furthermore, silencing lignin-associated *4CLs* can have different effects on syringyl-to-guaiacyl lignin (S/G) ratio depending on the species, ranging from increases in tobacco (*Nicotiana tabacum*; Kajita et al., 1996), Arabidopsis (*Arabidopsis thaliana*; Lee et al., 1997), and switchgrass (*Panicum virgatum*; Xu et al., 2011), to little change in alfalfa (*Medicago sativa*; Nakashima et al., 2008), to decreases in rice (*Oryza sativa*; Gui et al., 2011). Variable effects on S/G ratio have even been reported among closely related poplar species (Hu et al., 1999; Voelker et al., 2010; Chanoca et al., 2019 and references therein). Such variation has been attributed both to differing degrees of 4CL downregulation, as well as to 4CL multiplicity (Boerjan et al., 2003; Saballos et al., 2012). Analysis of knockout (KO) mutants should eliminate the uncertainty caused by partial gene silencing.

Arabidopsis, sorghum (*Sorghum bicolor*), and maize (*Zea mays*) *4cl* mutants showed preferential reductions in G-lignin, resulting in increased S/G ratios (Saballos et al., 2012; van Acker et al., 2013; Li et al., 2015; Xiong et al., 2019). Though rare until recently, transgenic nulls can now be efficiently obtained for genetically less tractable systems like woody perennials or polyploids using CRISPR/Cas9 technology (Voytas and Gao, 2014; Bewg et al., 2018). We previously reported that CRISPR-KO of the predominant lignin *4CL* in poplar led to a reduced S/G ratio (Zhou et al., 2015), whereas similar KO in tetraploid switchgrass increased the S/G ratio (Xu et al., 2011). This study aims to further characterize the poplar *4cl1* mutants by more comprehensive cell wall analysis, biomass saccharification, phenolic profiling, and RNA sequencing (RNA-seq). We present data to show distinct effects of *4CL*-KO on lignin biosynthesis and enzymatic hydrolysis of cell walls relative to *4cl* mutants of Arabidopsis and other herbaceous species. Our findings suggest that altered caffeic acid homeostasis along with altered expression of key lignin biosynthetic genes cooperatively sustain production of G-enriched lignin via the minor 4CL5 pathway in the *Populus* mutants.

RESULTS

4CL1-KO Preferentially Reduces S-Lignin Biosynthesis

We reported previously that CRISPR editing of *4CL1* in *P. tremula* × *alba* INRA 717-1B4 (hereafter "*4cl1* mutants") led to uniformly discolored wood and a 23% reduction in lignin content relative to wild-type and *Cas9*-only transgenic controls (hereafter "controls"), based on pyrolysis molecular beam mass spectrometry (pyMBMS) analysis (Zhou et al., 2015). Total lignin content determined by the Klason method revealed a 19% reduction in transgenic wood (Table 1). The pyMBMS analysis also detected a 30% decrease in the S/G ratio (Zhou et al., 2015), attributable to a sharp (34%) reduction of S-units, and a small (5%) though significant reduction of G-units (Table 1). Thioacidolysis showed a similar response in S-lignin, but a greater reduction (18%)

[1]This work was supported in part by the Institute of Food and Agriculture, United States Department of Agriculture (grant no. 2015–67013–22812), the Division of Integrative Organismal Systems (grant nos. IOS–1546867 and IOS–09223992), the Division of Biological Infrastructure (grant no. DBI–0421683) of the National Science Foundation, the BioEnergy Science Center (grant no. WPN–ERKP695), the Center for Bioenergy Innovation (grant no. WPN–ERKP886), and the Great Lakes Bioenergy Research Center (grant no. DE–SC0018409) funded by the Office of Biological and Environmental Research, Office of Science of the United States Department of Energy.

[2]Senior author.

[3]Author for contact: cjtsai@uga.edu.

[4]Present address: Department of Genetics and Genomics Sciences, Icahn School of Medicine at Mount Sinai, New York 10029

[5]Present address: Key Laboratory of Forest Genetics and Biotechnology, Co-Innovation Center for Sustainable Forestry in Southern China, College of Forestry, Nanjing Forestry University, Nanjing, Jiangsu 210037, China

[6]Present address: Department of Plant Biology, Ecology, and Evolution, Oklahoma State University, Stillwater, Oklahoma 74078

[7]Present address: State Key Laboratory of Subtropical Silviculture, Zhejiang Agriculture & Forestry University, Hangzhou, Zhejiang 310058, China

[8]Present address: Vlaams Instituut voor Biotechnologie Metabolomics Core, UGent-VIB Research Building, 9052 Ghent, Belgium

[9]Present address: Los Alamos National Laboratory, Los Alamos, New Mexico 87545

[10]Present address: Mascoma LLC (Lallemand Inc.), Lebanon, New Hampshire 03766

The author responsible for distribution of materials integral to the findings presented in this article in accordance with the policy described in the Instructions for Authors (www.plantphysiol.org) is: Chung-Jui Tsai (cjtsai@uga.edu).

X.Z. generated transgenic plants and measured Klason lignin; P.X. performed histology and amplicon sequencing; J.D. measured specific gravity and acoustic velocity; H.H., S.P., and M.G.H. performed glycome profiling analysis; B.N., R.N., and S.A.H. performed glycosyl composition analysis; S.A.H. measured crystalline cellulose content; G.G. and W.B. performed phenolic profiling analysis; E.G. and M.F.D. performed saccharification analysis through the BioEnergy Science Center; R.G. and J.R. performed nuclear magnetic resonance analysis and coordinated other cell wall analysis through the Great Lakes Bioenergy Research Center; L.-J.X. performed bioinformatic analysis; C.-J.T. conceived the project, analyzed data, and wrote the article with P.X. and S.A.H., with contributions from other authors.

[OPEN]Articles can be viewed without a subscription.

www.plantphysiol.org/cgi/doi/10.1104/pp.19.01550

Table 1. *Wood chemical properties of control and* 4cl1*-KO poplars*

Data represent means ± SE. Statistical significance was determined by two-sample Student's *t* test and indicated by bold-faced *P* values.

Cell Wall Composition	Control	*4cl1*	*P* Value	% Change
Klason lignin (% dry weight, $n = 7–9$)				
Total lignin content	15.94 ± 0.40	12.93 ± 0.37	<**0.001**	−19%
pyMBMS[a] (arbitrary units, $n = 7–12$)				
G	18.08 ± 0.17	17.18 ± 0.19	**0.006**	−5%
S	32.76 ± 0.21	21.60 ± 0.28	<**0.001**	−34%
S/G ratio	1.81 ± 0.02	1.26 ± 0.01	<**0.001**	−30%
Thioacidolysis (μmol/g Klason lignin, $n = 5$)				
H	29.15 ± 1.01	44.19 ± 1.20	<**0.001**	52%
G	1,146.37 ± 29.62	944.08 ± 26.45	<**0.001**	−18%
S	1,798.43 ± 53.37	1,180.51 ± 41.08	<**0.001**	−34%
S/G ratio	1.57 ± 0.02	1.25 ± 0.01	<**0.001**	−20%
Crystalline cellulose (% dry weight, $n = 8$)				
Glc	47.26 ± 0.42	45.85 ± 0.30	**0.016**	−3%
Hemicelluloses (% dry weight, $n = 5$)				
Ara	0.29 ± 0.01	0.33 ± 0.01	**0.032**	15%
Rha	0.48 ± 0.01	0.49 ± 0.00	0.062	3%
Xyl	14.12 ± 0.19	15.09 ± 0.13	**0.003**	7%
Man	0.95 ± 0.02	0.70 ± 0.02	<**0.001**	−26%
Gal	0.65 ± 0.03	0.60 ± 0.02	0.190	−8%
Glc	4.03 ± 0.17	3.77 ± 0.16	0.290	−6%
Glycosyl composition (mol%, $n = 5–6$)				
Ara	1.02 ± 0.06	1.12 ± 0.04	0.169	10%
Rha	1.97 ± 0.08	2.00 ± 0.10	0.796	2%
Fuc	0.12 ± 0.02	0.17 ± 0.02	0.092	42%
Xyl	60.05 ± 1.42	61.65 ± 1.96	0.471	3%
GlcA	1.98 ± 0.07	2.30 ± 0.11	**0.035**	16%
OMe-GlcA	0.58 ± 0.04	0.83 ± 0.09	**0.019**	43%
GalA	3.50 ± 0.14	4.47 ± 0.30	**0.013**	28%
Man	1.37 ± 0.03	1.03 ± 0.09	**0.002**	−25%
Gal	3.47 ± 0.38	2.80 ± 0.12	0.123	−19%
Glc	25.88 ± 1.34	23.65 ± 2.00	0.320	−9%

[a]pyMBMS data were from Zhou et al. (2015).

of G-lignin, in addition to a 52% increase of the minor component, H-lignin (Table 1), which is poorly pyrolyzed and hence undetectable using pyMBMS (Sykes et al., 2015). To probe the structural modifications in walls of the mutant further, two-dimensional nuclear magnetic resonance (NMR) analysis was performed using both whole cell wall residues and cellulolytic enzyme lignins. The results were highly concordant with those of pyMBMS and thioacidolysis, showing a ~30% decrease in S/G ratio along with increased H-lignin in the mutants (Fig. 1). The frequency of *p*-hydroxybenzoate units also increased in the mutants (Fig. 1), but we do not see evidence for the appearance of (higher levels of) β–β-coupling products derived from monolignol (largely sinapyl) *p*-hydroxybenzoate conjugates to produce tetrahydrofurans rather than the familiar resinols derived from unconjugated monolignols, as has been observed in palms (*Elaeis guineensis*; Lu et al., 2015). Taken together, all analytical methods employed in this study showed consistent decreases of S/G ratio by 20% to 30% in the *4cl1* mutants, resulting from a preferential reduction of S-lignin.

Phloroglucinol staining of stem cross sections confirmed reduced lignification in the mutants (Fig. 2, A and B). In agreement with previous findings (Coleman et al., 2008; Voelker et al., 2010), reduced lignin accrual led to collapsed xylem vessels (Fig. 2, A and C, versus B and D). Accordingly, wood specific gravity was significantly reduced in *4cl1* mutants (Fig. 2E). The mutants also exhibited significantly lower acoustic velocity (Fig. 2F), which is correlated with the microfibril angle of the S2 layer (Schimleck et al., 2019). No other apparent growth anomaly was observed under greenhouse conditions. It appears that the effects on poplar growth by targeted KO of *4CL1* were smaller than those reported previously by inherently less specific antisense downregulation (Voelker et al., 2010). Further evaluation under field conditions would be necessary to assess the impact of lignin alteration on mutant growth.

4CL1-KO Has No Obvious Effects on Biomass Saccharification

Reduction of lignin content, regardless of S/G change, has been shown to improve enzymatic sugar release in alfalfa, Arabidopsis, and poplar (Chen and Dixon, 2007; Mansfield et al., 2012a; van Acker et al., 2013;

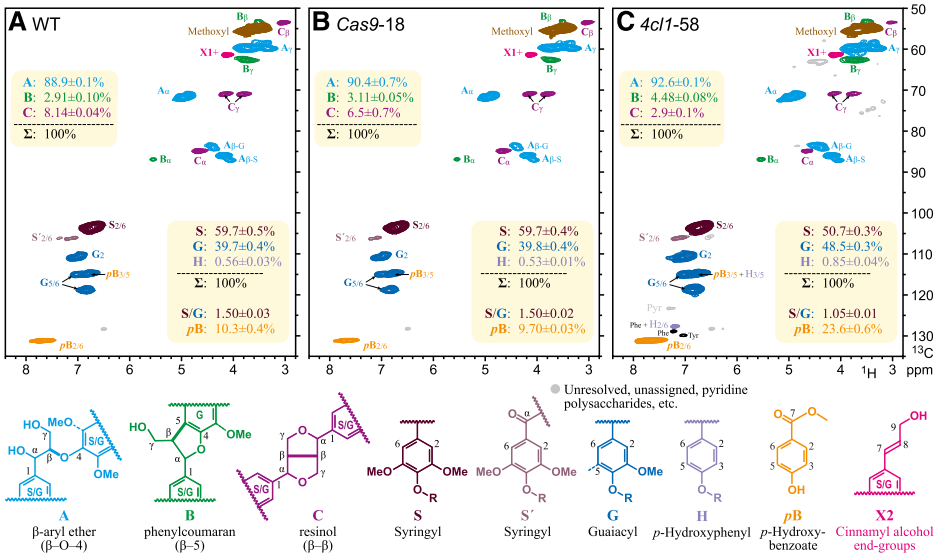

Figure 1. NMR analysis of *4cl1* mutant and control poplar wood. Representative ^{1}H–^{13}C heteronuclear single-quantum coherence correlation spectra of the aromatic region of enzyme lignins from ball-milled wood samples. A to C, Wild type (A), *Cas9* (B), and *4cl1* mutant (C). The main lignin structures and linkages identified are illustrated below and color-coded to match their assignments in the spectra. Volume integrals (with the same color coding) were measured using the α-C/H correlation peaks from A-, B-, and C-units, and $S_{2/6}$ + $S'_{2/6}$, G2, and $H_{2/6}$ (corrected for Phe) aromatics (with the integrals halved as usual for the S-, H-, and C-units) are noted as the mean ± SE of biological replicates (n = 3 for wild type, 2 for *Cas9*, and 5 for *4cl1*; Kim and Ralph, 2010; Mansfield et al., 2012b). Note that the interunit linkage distribution (A:B:C) is determined from volume integrals of just those units and made to total 100%; small differences (such as the apparently enhanced β-ether A-level in the *4cl1* line) should not be overinterpreted, as we were unable to delineate authenticated peaks for, nor therefore obtain reliable accounting of, various tetrahydrofurans (from β–β-coupling of monolignol *p*-hydroxybenzoates), nor of the 4–*O*–5- and 5–5-linked units that require one or two G-units (and would therefore logically be higher in the *4cl1* lines, with their higher %G-units). Also note that the H-unit ($H_{2/6}$) correlation peak overlaps with another peak from Phe protein units (Kim et al., 2017); integrals were corrected by subtracting the integral from the resolved Phe peak below it to obtain the best estimate available.

Wang et al., 2018). Unexpectedly, we found no difference between control poplar and *4cl1* mutants in enzymatic Glc and Xyl release after hydrothermal pretreatment (Fig. 2G) using the high-throughput recalcitrance assay developed by the U.S. Department of Energy-funded BioEnergy Science Center (BESC; Selig et al., 2010). Independent analyses using the high-throughput method of the Department of Energy-Great Lakes Bioenergy Research Center (GLBRC; Santoro et al., 2010) also detected no differences in Glc release (Fig. 2G). Mutant samples released slightly higher levels of Xyl, but only after less severe (hot water and dilute acid, not alkaline) pretreatments (Fig. 2G). The overall lower sugar yields from the GLBRC assays are similar to those reported elsewhere (Wilkerson et al., 2014), and reflect the milder pretreatment and enzymatic hydrolysis conditions than those applied with the BESC methods (Santoro et al., 2010; Selig et al., 2010).

Altered Lignin-Carbohydrate Interactions in the Cell Wall of *4cl1* Mutants

As lignin is purportedly cross linked with cell wall polysaccharides, we next examined the *4CL1*-KO effects on cell wall glycans and their interaction with lignin. We detected a small decrease in crystalline cellulose contents of the mutants (Table 1). Monosaccharides typically associated with hemicelluloses showed slight changes, with Man decreasing significantly, and the most abundant Xyl increasing slightly (Table 1). Glycosyl residue composition analysis further revealed increased mol% of GlcA, its 4-O-methylated form, and GalUA, the main component of pectins (Table 1). These data suggest altered cell wall polysaccharide composition in lignin-reduced *4cl1* mutants.

Extractive-free wood meals were then subjected to cell wall fractionation to provide a finer resolution analysis of matrix polysaccharide organization by glycome profiling using a panel of cell wall glycan-directed monoclonal antibodies (mAbs; Pattathil et al., 2010, 2012). The amounts of extractable cell wall material differed little between control and *4cl1* mutants (Supplemental Fig. S2A). The glycan epitope profiles from cell wall fractions enriched with pectins (oxalate and carbonate extracts) and hemicelluloses (1 and 4 M KOH extracts) were largely similar between genotypes, with a few epitopes exhibiting slightly lower signals in the mutants (Fig. 3; Supplemental Fig. S2B). In contrast, we observed significantly increased polysaccharide extractability in the chlorite fraction of mutant cell walls (Fig. 3), especially

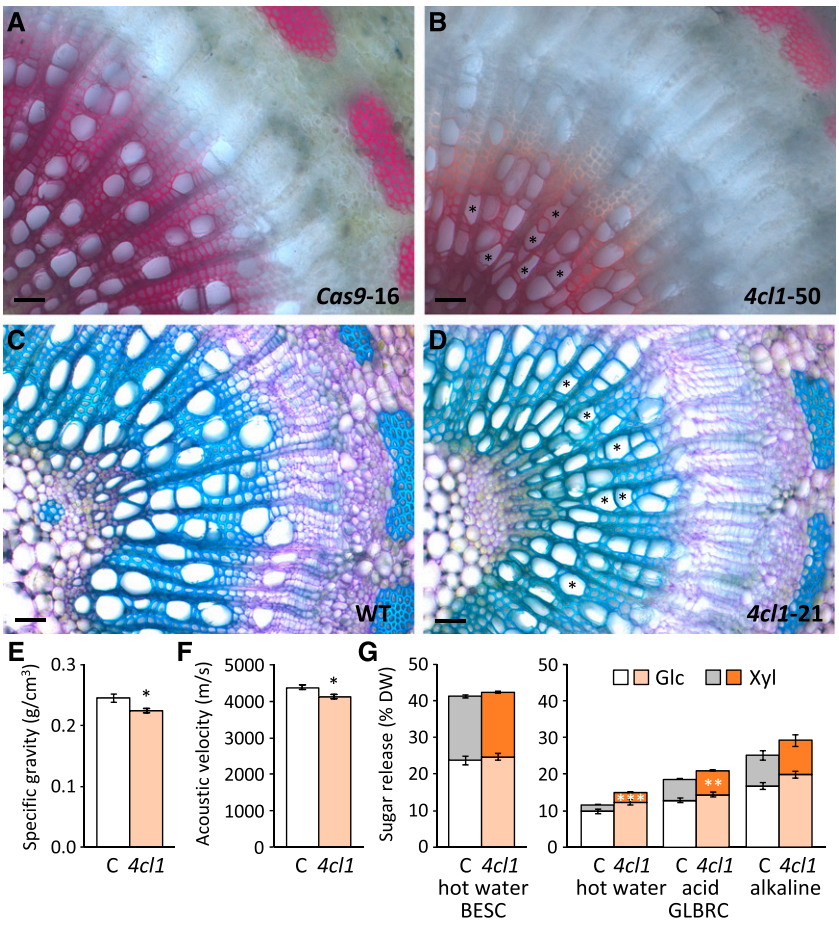

Figure 2. Histology, physical properties, and saccharification of mutant and control poplar wood. A and B, Stem cross sections (10th internode) stained with phloroglucinol. C and D, Stem cross sections (8th internode) stained with toluidine blue. Representative images from control (wild type or *Cas9*) and *4cl1* mutant lines are shown. Collapsed vessels are marked with asterisks. Scale bars = 50 μm. E and F, Wood-specific gravity (E) and acoustic velocity (F) of control (n = 9) and *4cl1* (n = 12) samples. G, Enzymatic sugar release of control and mutant samples after BESC hydrothermal (n = 6) and GLBRC hydrothermal, dilute acid, and dilute alkaline pretreatments (n = 5). Data in E to H represent means ± SE. Statistical significance was determined by Student's t test ($^{***}P < 0.001$; $^{**}P < 0.01$; and $^{*}P < 0.05$).

for epitopes recognized by mAb groups 4-*O*-methyl GlcA-substituted xylans (Xylan-5), linear unsubstituted xylans (Xylan-6/Xylan-7), rhamnogalacturonan I, arabinogalactan, and pectic (rhamnogalacturonan I and homogalacturonan) backbones (Pattathil et al., 2010; Schmidt et al., 2015; Ruprecht et al., 2017). Because chlorite degrades lignin and liberates lignin-bound glycans, the enhanced carbohydrate extractability in the chlorite fraction is consistent with less interaction between matrix polysaccharides and lignin in the mutant cell wall. Whether the increased release of those glycans reflects reduced lignin abundance and/or altered lignin composition was not determined.

Altered Phenylpropanoid Metabolism in *4cl1* Mutants

Ultra performance liquid chromatography-mass spectrometry profiling of methanolic extracts from developing xylem revealed a major shift in phenylpropanoid metabolism in the mutants. Consistent with decreased lignin biosynthesis, various oligolignols and their hexosides were detected at drastically reduced levels in the mutants (Table 2). Also significantly reduced were lignin pathway intermediates 4-coumaroyl and caffeoyl shikimate esters (Table 2), whose synthesis depends on 4CL-activated hydroxycinnamoyl-CoAs as acyl donors (Hoffmann et al., 2003). Among potential 4CL substrates, caffeic acid is the only hydroxycinnamic acid consistently detected in control xylem under our experimental conditions (Table 2). The *4cl1* mutants accrued elevated levels of caffeic acid and its sulfate ester, along with very high levels of phenolic hexose esters and hexosides (Table 2). In particular, a caffeic acid 3/4-*O*-hexoside increased by nearly 80-fold and became the most abundant soluble phenylpropanoid identified in the mutant xylem extracts (Table 2). Mutants also contained detectable levels of 4-coumaric acid and ferulic acid sulfate, as well as highly increased hexose conjugates of 4-coumarate, ferulate, and sinapate (Table 2). Chlorogenic acid (5-*O*-caffeoyl quinate), the predominant hydroxycinnamoyl quinate ester in poplar, changed little in the mutants, whereas the less abundant 3-*O*-caffeoyl quinate, 3-*O*-feruloyl quinate, and 4-*O*-feruloyl quinate increased significantly (Table 2). It appears that, unlike for the shikimate conjugates, synthesis of hydroxycinnamoyl quinate esters in poplar is largely independent of 4CL1. Together, the phenolic profiling data revealed a buildup of hydroxycinnamates and their diversion into nonstructural phenylpropanoid pools at the expense of lignin precursors in the *4cl1* mutants.

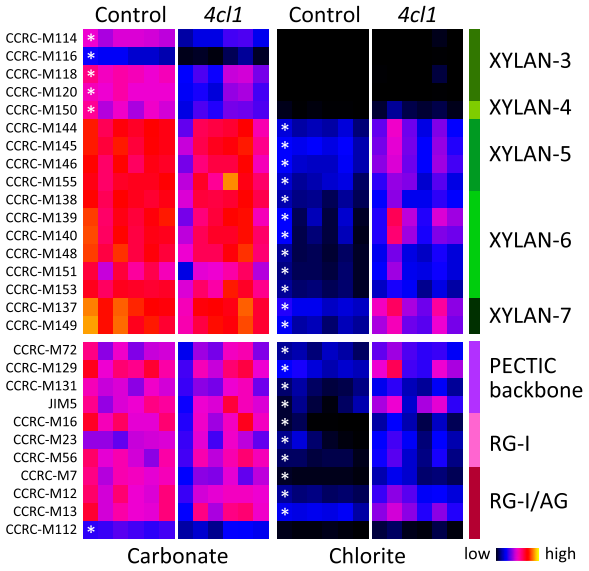

Figure 3. Glycome profiling of *4cl1* mutant and control poplar wood. Heatmap depiction of signal intensities resulting from binding of cell wall glycan-directed mAbs to two cell wall fractions extracted by sodium carbonate and chlorite from control and mutant samples. mAbs are arranged in rows by the cell wall glycan epitope groups (denoted by vertical color bars on the right), and biological replicates ($n = 6$) are shown in columns. Asterisks indicate significant differences between plant groups determined by Student's *t* test ($P < 0.01$, fold-change ≥ 1.5).

Transcriptional Adjustments of Lignin Biosynthesis

RNA-seq analysis of developing xylem tissues from six representative mutants and six controls (three wild-type and three *Cas9* controls) identified 1,752 genes with significantly altered transcript abundance in response to *4CL1*-KO, approximately two-thirds of which were upregulated (1,153) and the remaining (599) downregulated. Because guide RNA (gRNA)-directed CRISPR/Cas9 mutations are located in the first exon of Pta*4CL1* (Zhou et al., 2015), aberrant transcripts containing premature stop codons resulting from frameshift indels (Supplemental Table S1) would produce nonfunctional proteins in the mutants. In addition, the aberrant transcripts are potential targets for nonsense-mediated mRNA decay (Conti and Izaurralde, 2005). Accordingly, *4CL1* was among the most significantly downregulated genes in the mutants, with its (aberrant) transcript levels decreased by 92% (Fig. 4A). Our data thus underscore the efficacy of CRISPR/Cas9 mutagenesis at multiple levels, affecting steady-state transcript accumulation as well as protein function.

Transcript levels of many lignin biosynthetic genes, including *4CL1* paralog *4CL5*, were not significantly changed in the *4cl1* mutants. However, the genome duplicates *F5H1* and *F5H2* encoding ferulate/coniferaldehyde 5-hydroxylases were significantly downregulated, and they are the only known monolignol pathway genes besides *4CL1* to show such patterns (Fig. 4A). As F5Hs occupy the branch-point into S-lignin biosynthesis, their downregulation is consistent with the preferential reduction of S-lignin in *4cl1* mutants. Other genes implicated in lignification, including a UDP-glycosyltransferase (Potri.014G096100) orthologous to Arabidopsis UGT72B1 involved in monolignol glycosylation (Lin et al., 2016) and a laccase (Potri.010G193100) involved in oxidative coupling of monolignols (Ranocha et al., 2002; Lu et al., 2013), were also downregulated in the mutants (Fig. 4A). In contrast, transcript levels of two lignin genes increased significantly, and they encode enzymes acting immediately upstream (caffeoyl shikimate esterase, CSE1) and downstream (caffeoyl-CoA *O*-methyltransferase, CCoAOMT1) of the 4CL reaction with caffeic acid. Both enzymes are encoded by genome duplicates with similar expression levels in poplar xylem and, in both cases, only one copy each was affected in the *4cl1* mutants (Fig. 4A). This suggests involvement of CSE1 and CCoAOMT1 in homeostatic regulation of caffeic acid and caffeoyl-CoA in response to *4CL1*-KO. Recently, a cytosolic ascorbate peroxidase (APX) was shown to possess 4-coumarate 3-hydroxylase (C3H) activity and to convert 4-coumaric acid to caffeic acid in both monocots and dicots, supporting an alternative route in lignin biosynthesis involving free phenolic acids (Barros et al., 2019). Two putative orthologs of this dual-function APX-C3H are present in the poplar genome, and one of them (Potri.009G015400, APX-C3H1) was significantly upregulated in the mutants (Fig. 4A). Although catalytic properties remain to be confirmed, upregulation of the putative poplar *APX-C3H1* may also contribute to elevated accumulation of caffeic acid and its derivatives.

Cell Wall Remodeling and Detoxification Responses in the *4cl1* Mutants

Genes downregulated in the KO mutants showed an overrepresentation of gene-ontology (GO) terms associated with cell wall biogenesis and polysaccharide biosynthesis (Fig. 4C). Examples include transcription factors (TFs), such as top-level wood-associated NAC-domain (WND) proteins, WND1A and WND5A, and downstream TFs, NAC154, NAC156, MYB10, MYB128, MYB167, and MYB221, that regulate lignin, cellulose, and xylan biosynthesis (Ye and Zhong, 2015; Fig. 4A). There was widespread downregulation of genes involved in the biosynthesis of all major cell wall glycans, including cellulose, xylans, and pectins (Fig. 4A). In contrast, genes encoding cell wall-modifying enzymes or cell wall-loosening proteins were significantly upregulated (Fig. 4B). The results are consistent with the altered cell wall polysaccharide composition and extractability, and provide molecular bases for cell wall remodeling as a result of impaired lignification in the mutants.

GO categories associated with detoxification, sulfur assimilation, and oxidation-reduction processes were over-represented among genes upregulated in the mutants (Fig. 4C). Of particular interest are genes

Table 2. *Xylem phenolic metabolites with significantly altered abundance in* 4cl1 *mutants*

Data represent mean signal intensities ± SE of $n = 10$ control (three wild-type and seven Cas9 vector control lines) or 14 *4cl1*-KO lines. Only data with signal intensities ≥ 1,000 in at least one group (except *), significant differences ($P < 0.002$) between groups based on Student's *t* test (except **), and confirmed peak annotation are shown. The exceptions are included for reference.

Name	Retention Time	*m/z*	Ion	Control	*4c1*	Fold Change
Oligolignol						
G(8-*O*-4)G 9-*O*-Hexoside	7.15	537.1995	M-H	1,820 ± 123	47 ± 22	−39
G(8-*O*-4)G Hexoside	7.44	537.1995	M-H	7,153 ± 430	1,406 ± 167	−5.1
G(8-*O*-4)G(8-*O*-4)G	9.94	571.2202	M-H	3,242 ± 190	3 ± 2	−1,064
Gox(8-*O*-4)G	11.92	373.1307	M-H	1,321 ± 70	12 ± 4	−110
G(8-5)G [$-H_2O$]	13.24	339.1250	M-H	2,049 ± 181	23 ± 10	−89
G(8-*O*-4)S(8-5)G	14.95	583.2209	M-H	6,137 ± 402	65 ± 49	−94
G(8-*O*-4)S(8-5)G	15.77	583.2205	M-H	1,264 ± 154	2 ± 1	−641
Hydroxycinnamoyl shikimate						
4-Coumaroyl shikimate	9.72	319.0841	M-H	17,617 ± 4,276	4,658 ± 734	−3.8
Caffeoyl shikimate	6.28	335.0822	M-H	79,601 ± 16,211	16,973 ± 1,928	−4.7
Caffeoyl shikimate	7.78	335.0791	M-H	16,415 ± 2,815	2,844 ± 324	−5.8
Feruloyl shikimate	10.31	349.0942	M-H	682 ± 140	23 ± 10	−30
Phenolic acid						
4-Coumaric acid*	7.96	163.0399	M-H	41 ± 13	760 ± 114	19
Caffeic acid	5.04	179.0352	M-H	1,110 ± 121	3,404 ± 389	3.1
Caffeic acid sulfate	1.82	258.9947	M-H	1,392 ± 138	4,650 ± 254	3.3
Ferulic acid sulfate	5.07	273.0085	M-H	0 ± 0	3,912 ± 315	∞
Phenolic acid hexose/hexoside						
4-Coumaroyl hexose	4.64	325.0996	M-H	2,876 ± 431	212,766 ± 15,741	74
4-Coumaroyl hexose	5.21	325.0985	M-H	1,994 ± 334	88,055 ± 5,699	44
Caffeoyl hexose	3.43	341.0931	M-H	224 ± 103	13,415 ± 936	60
Caffeic acid 3/4-*O*-hexoside	4.13	341.0946	M-H	7,950 ± 649	611,832 ± 22,149	77
Caffeic acid 3/4-*O*-hexoside	5.61	341.0937	M-H	6,539 ± 302	205,906 ± 12,360	32
Ferulic acid 4-*O*-hexoside	3.83	711.2309	2M-H	117 ± 56	209,459 ± 10,490	1,798
Feruloyl hexose	5.46	355.1104	M-H	1,539 ± 415	184,710 ± 11,173	120
Feruloyl hexose	5.54	711.2215	2M-H	0 ± 0	32,748 ± 3,070	∞
Feruloyl hexose	5.96	355.1093	M-H	266 ± 144	38,777 ± 3,127	146
Sinapic acid 4-*O*-hexoside	4.49	771.2552	2M-H	1,463 ± 217	263,304 ± 8,064	180
Sinapic acid 4-*O*-hexoside	6.21	385.1179	M-H	1,091 ± 89	78,135 ± 5,624	72
4-Hydroxybenzoyl hexose	2.74	299.0824	M-H	4,356 ± 426	95,399 ± 9,034	22
Vanillic acid 4-*O*-hexoside	2.30	659.1967	2M-H	9,322 ± 313	363,392 ± 13,301	39
Hydroxycinnamoyl quinate						
3-*O*-Caffeoyl quinate	3.11	353.0889	M-H	2,001 ± 284	7,236 ± 833	3.6
3-*O*-Feruloyl quinate	4.83	367.1046	M-H	1,026 ± 127	2,665 ± 341	2.6
4-*O*-Feruloyl quinate	6.83	367.1047	M-H	393 ± 85	1,746 ± 194	4.4
5-*O*-Caffeoyl quinate*	4.32	353.0911	M-H	21,688 ± 2,000	28,126 ± 2,621	1.3
4-*O*-Caffeoyl quinate**	4.69	353.0893	M-H	2,283 ± 220	2,630 ± 266	1.2

involved in sulfur assimilation into Cys for synthesis of other sulfur-containing compounds, including glutathione. Upregulation of genes encoding glutathione *S*-transferases (GSTs), redox-active proteins, and enzymes in the glutathione-ascorbate cycle underscores the likelihood of redox adjustments in the mutants (Fig. 5).

Conditional Involvement of *4CL5* in Lignin Biosynthesis

The *4cl1* mutants somehow accrue ~80% of wild-type lignin levels (Table 1), even though *4CL1* transcripts normally comprise >80% of xylem-expressed *4CL* transcript levels in poplar (Supplemental Fig. S1). The only other xylem-expressed 4CL isoform, 4CL5, must therefore sustain lignin biosynthesis in the absence of 4CL1. Interestingly, CRISPR-KO of *4CL5* did not change either lignin content or S/G ratio of the stem wood (Supplemental Fig. S3), suggesting only a minor or conditional role in lignification under normal growth conditions. As *4CL5* transcript abundance was not significantly altered in the *4cl1* mutants (Fig. 4A), other mechanism(s) must exist for in vivo enhancement of its function. We constructed genotype-specific xylem gene coexpression networks (see "Materials and Methods") to compare the expression contexts of *4CL1* and *4CL5*, and their shifts in response to *4CL1*-KO (Supplemental Fig. S4). The wild-type network placed *PAL2* and *4CL1* along with *NAC154* and *MYB128* in the brown module, *4CL5* and *APX-C3H1* in the yellow module, and *PAL5*, *CSE1*, *CCoAOMT1*, *F5H1*, and *F5H2* along with *MYB167* and *MYB221* in the

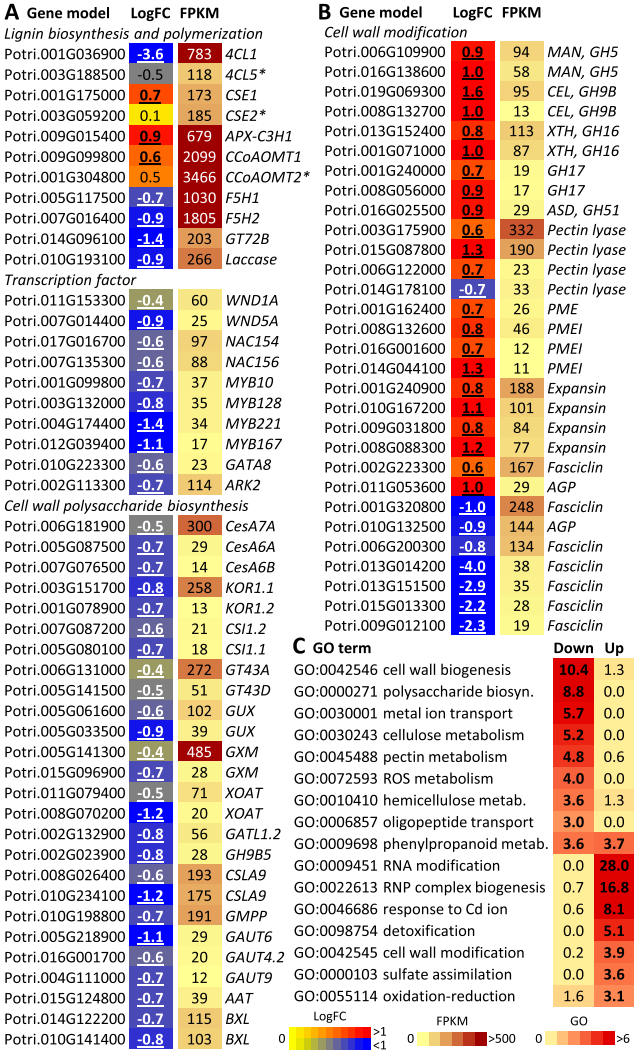

Figure 4. Transcriptional responses of *4cl1* mutants. A, Expression response heatmaps of genes involved in cell wall biogenesis. B, Expression response heatmaps of genes involved in cell wall remodeling. LogFC, $\log_2$-transformed fold-change (mutant/control) values; fragments per kilobase of transcript per million mapped reads (FPKMs), average transcript abundances of control samples. Only genes with significant differences ($Q \leq 0.01$, boldface and underlined) and with control FPKM ≥ 10 are shown, except for genome duplicates marked with asterisks. C, GO enrichment of differentially up- or downregulated genes in the mutants. Representative GO terms are shown with the negative $\log_{10}$-transformed *P* values. Heatmaps are visualized according to the color scales at the bottom. *AAT*, arabinosyltransferase; *AGP*, arabinogalactan protein; *ARK*, ARBORKNOX; *ASD*, arabinofuranosidase; *BXL*, β-xylosidases/α-arabinofuranosidase; *CCoAOMT*, caffeoyl-CoA O-methyl-transferase; *CEL*, cellulase; *CesA*, cellulose synthase; *CSI*, cellulose synthase interacting protein, *CSLA*, mannan synthase; *F5H*, ferulate 5-hydroxylase; *GATL*, galacturonosyltransferase–like; *GAUT*, galacturonosyltransferases; *GH*, glycosyl hydrolase; *GH9B*, class B endoglucanase; *GMPP*, GDP-Man pyrophosphorylase; *GT*, glycosyltransferase; *GT43*, xylan xylosyltransferase; *GUX*, glucuronyltransferase; *GXM*, glucuronoxylan O-methyltransferase; *KOR*, KORRIGAN; *MAN*, mannase; *PME(I)*, pectin methyl-esterase (inhibitor); *XOAT*, xylan *O*-acetyltransferase; *XTH*, xyloglucan endotransglucosylase.

turquoise module (Fig. 6; Supplemental Dataset S1). In the *4cl1*-KO network, *4CL1*, *CCoAOMT2*, *F5H1*, *F5H2*, *NAC154*, *MYB128*, and *MYB167* were assigned to the turquoise module, and *PAL2*, *PAL5*, *4CL5*, *CSE1*, and *CCoAOMT1* to the blue module (Fig. 6; Supplemental Dataset S1). The data support distinct regulation of *4CL1* and *4CL5*, and suggest transcriptional rewiring of *4CL5*, *CSE1*, and *CCoAOMT1* to the same coexpression module as part of a compensatory response to sustain lignification in the *4cl1* mutants.

DISCUSSION

4CL-KO Effects on Lignin Composition and Enzymatic Hydrolysis Differ between Poplar and Herbaceous Species

The cell-wall polymer lignin provides structural integrity and protection to plants (Weng and Chapple, 2010). Its abundance and structural complexity, however, render it a negative factor in forage quality and inhibit its removal in cellulosic biomass utilization for pulping and biofuels production (Boerjan et al., 2003). Studies with wild poplar populations (Studer et al., 2011), sorghum and maize *brown midrib* mutants

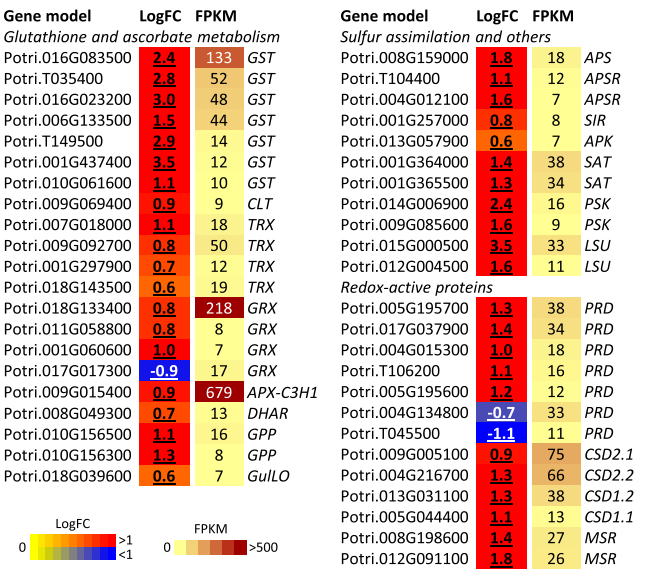

Figure 5. Transcriptional responses of detoxification genes in the mutants. Expression response heatmaps of genes associated with glutathione-ascorbate metabolism, sulfur assimilation, and antioxidant systems. Data presentation is the same as Figure 4. Only genes with control fragments per kilobase of transcript per million mapped reads (FPKM) ≥ 5 (or ≥ 10 in the case of *GSTs* and *PRDs*) are shown. *APK*, adenosine-phosphosulfate kinase; *APS*, ATP sulfurylase; *APSR*, adenosine-phosphosulfate reductase; *CLT*, chloroquine-resistance-like (glutathione) transporter; *CSD*, Cu/Zn superoxide dismutase; *DHAR*, dehydroascorbate reductase; *GPP*, Gal-1-phosphate phosphatase; *GRX*, glutaredoxin; *GulLO*, gulonolactone oxidase; *LSU*, response to low sulfur; *MSR*, Met sulfoxide reductases; *PRD*, peroxidase; *PSK*, phytosulfokine; *SAT*, Ser acetyltransferase; *SIR*, sulfite reductase; *TRX*, thioredoxin.

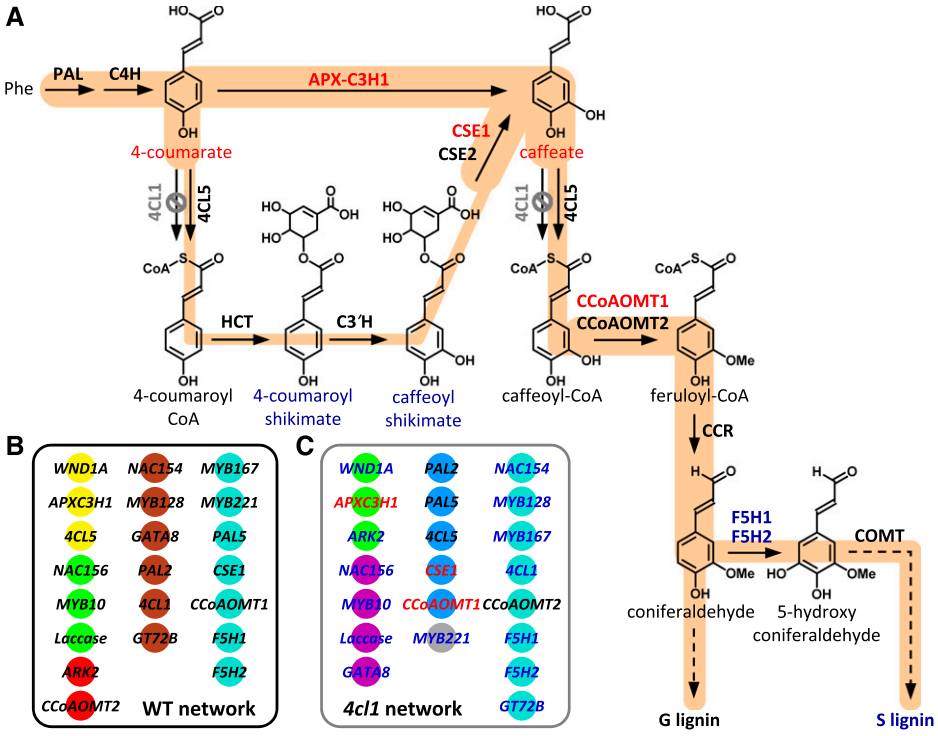

Figure 6. Schematic of the transcriptional and metabolic adjustments of lignin biosynthesis in *4cl1* mutants. A, The major monolignol biosynthetic routes are shown with relevant pathway steps and intermediates discussed in this study. Red and blue fonts indicate higher and lower abundances, respectively, in the *4cl1* mutants. The slightly reduced G-lignin is shown in black to contrast with the drastically reduced S-lignin in blue. Orange background shading depicts the pathway flows, with thickness representing relative transcript and metabolite level changes detected in the mutants. B and C, Coexpression module assignments for lignin pathway genes and TFs in control (B) and mutant (C) networks. Genes are arranged and color-coded by modules they were assigned to, and red and blue text in C indicates up- or downregulation in the mutants, respectively. Abbreviations are the same as in Figure 4.

(Saballos et al., 2008; Xiong et al., 2019), Arabidopsis T-DNA mutants (van Acker et al., 2013), and transgenic alfalfa and poplar (Chen and Dixon, 2007; Mansfield et al., 2012a; Wang et al., 2018) have reported a major, and negative, effect of lignin content on enzymatic sugar release, with lignin S/G ratio playing a minor role. For instance, KO of lignin-associated *4CL* led to reduced lignin content and improved enzymatic saccharification in Arabidopsis, maize, sorghum, and switchgrass (Saballos et al., 2008; Van Acker et al., 2013; Park et al., 2017; Xiong et al., 2019). However, for the poplar *4cl1* mutants investigated here, similar degrees of lignin reduction had at best negligible effects on sugar release by multiple pretreatment methods (Fig. 2, G and H). The S/G ratio was reduced by ~30% in poplar mutants due to drastically reduced S-lignin abundance (Table 1), but was increased in Arabidopsis, switchgrass, sorghum, and maize mutants owing to strong reductions of G-lignin contents (Saballos et al., 2008; van Acker et al., 2013; Park et al., 2017; Xiong et al., 2019). Poplars and other angiosperm trees with significant secondary growth typically contain S-rich lignin (S/G > 1.5), whereas herbaceous species are usually G-rich (e.g. Sun et al., 2012). The biased effects of *4CL*-KO on S- and G-lignin flux of woody and herbaceous species therefore seem to track with canalized taxonomic determinants of lignin S/G ratio. S-lignin is known to be associated with more chemically labile linkages and to possess a higher reactivity during pulping as well as various biomass pretreatment regimes (Studer et al., 2011; Mansfield et al., 2012a). It thus appears that the potential gain in enzymatic hydrolysis brought about by reduced lignin was offset by decreased S/G ratio in the poplar *4cl1* mutants. We interpret these results to suggest that lignin reduction predominantly in the form of S-units does not improve biomass saccharification.

Transcriptional and Metabolic Coordination Enables 4CL5 Compensation

Plasticity in the lignin biosynthetic pathway as evidenced by multiple possible routes (Fig. 6; Barros et al., 2019) may accommodate developmental, environmental, or species-dependent variations in lignification. 4CLs, for instance, can utilize multiple hydroxycinnamate substrates in vitro, but how substrate utilization is regulated in vivo is largely unknown. 4CL activation of 4-coumarate is obligatory for production of the downstream intermediates, 4-coumaroyl and caffeoyl shikimate esters, in lignin biosynthesis (Schoch et al., 2001; Hoffmann et al., 2004; Coleman et al., 2008), and this was confirmed by greatly depleted shikimate ester levels in the *4cl1* mutants (Table 2). Like many Class-I 4CLs involved in lignin biosynthesis, poplar 4CL1 also utilizes caffeic acid, which is the most abundant free hydroxycinnamate in poplar xylem (Harding et al., 2002; Chen et al., 2013; Table 2). The significant increases of free caffeic acid and its hexose conjugates in the mutant xylem are consistent with a substrate buildup due to impaired 4CL1 conversion. Caffeic acid accrual can also be attributed to conversion from surplus 4-coumaric acid, another 4CL1 substrate, by the upregulated APX-C3H1, as well as from residual caffeoyl shikimate via CSE1. No incorporation of caffeates or caffeoyl alcohol into the lignin

polymer was evident in the NMR spectra (even at levels nearer the baseplane than those plotted in Fig. 1). Besides the reduced S/G ratio and consequent changes in the interunit linkage distribution that were largely as expected, and the elevation of *p*-hydroxybenzoate levels, there were no other evident structural changes in the *4cl1* lignin, and no obviously new components as has often been observed in mutants and transgenics (Ralph and Landucci, 2010).

Several lines of evidence suggest that increased caffeic acid accrual in the *4cl1* mutants was not merely due to precursor buildup, but to a tightly regulated compensatory mechanism to sustain lignification. (1) The *4cl1* mutants exhibit ~20% lignin reduction; that the reduction is not more severe means that substantial levels of lignin biosynthesis must be upheld by 4CL5, the remaining xylem isoform. (2) Xylem transcript and protein abundances of 4CL5 are several-fold lower than those of 4CL1 (Fig. 4A; Wang et al., 2018). (3) *4CL1* and *4CL5* exhibited distinct coexpression patterns with other genes and TFs implicated in lignin biosynthesis (Fig. 6). These, along with the silent lignin phenotype of *4cl5* mutants during normal growth (Supplemental Fig. S2), all point to 4CL5's conditional involvement in lignin biosynthesis under specific circumstances. (4) All three lignin genes upregulated in the *4cl1* mutants, *CSE1*, *APX-C3H1*, and *CCoAOMT1*, occupy pathway steps immediately upstream and downstream of caffeic acid-to-caffeoyl-CoA activation (Fig. 6). This is in sharp contrast to Arabidopsis *4cl1* mutants, in which significant upregulation of early pathway genes *AtPAL2*, *AtC4H*, and *AtC3'H* was reported (Vanholme et al., 2012). Our finding that *4CL5*, *CSE1*, and *CCoAOMT1* belonged to the same coexpression module in the *4cl1*-specific network highlights a specific involvement of *CSE1* and *CCoAOMT1* in the distinct lignin compositional changes in the poplar *4cl1* mutants. Elevated *CSE1* expression would be expected to direct residual lignin biosynthetic pathway fluxes toward caffeic acid, while also relieving the buildup of potential 4CL inhibitors, 4-coumaroyl and caffeoyl shikimates (Lin et al., 2015), in the process. The increased supply of caffeic acid would be necessary for 4CL5 catalysis to commence because its estimated K_m value is several-fold higher than that of the predominant 4CL1 (Chen et al., 2013). The observed 3-fold increase in free caffeic acid levels in the *4cl1* mutants is in general agreement with this scenario. Upregulation of the downstream *CCoAOMT1* could further drive the caffeate-to-caffeoyl-CoA flux toward lignification. This, along with caffeic acid glycosylation, could prevent overaccumulation of caffeic acid that may cause substrate self-inhibition of 4CL5 (Chen et al., 2013). Thus, transcriptional coactivation of *CSE1* and *CCoAOMT1* in effect altered the biochemical milieu, enabling the low-affinity 4CL5 to engage in a compensatory function to sustain lignification, even though *4CL5* expression was not increased in the *4cl1* mutants. Regardless, the 4CL5 pathway was not very efficient and could only partially restore lignification in the *4cl1* mutants. We further argue that the 4CL5 compensatory pathway is primarily channeled toward G-lignin biosynthesis due to downregulation of *F5H* paralogs. The data thus provide a mechanistic basis for the biased effect on S-lignin accrual in the poplar *4cl1* mutants.

Crosstalk among Lignification, Redox Regulation, and Sulfur Metabolism

The two lignin biosynthetic enzymes APX-C3H1 and CSE1 involved in caffeic acid synthesis both possess additional functions associated with detoxification of hydrogen peroxide, lipid peroxides, and superoxide (Gao et al., 2010; Barros et al., 2019). Their upregulation in *4cl1* mutants coincided with induction of *GSTs*, *PRDs*, *CSDs*, *MSRs*, and genes encoding enzymes of the glutathione-ascorbate cycle, all of which have been implicated in scavenging of reactive oxygen species (Rouhier et al., 2008; Molina-Rueda et al., 2013; Rey and Tarrago, 2018). Coordinated regulation of multiple antioxidant systems may be crucial to maintain redox balance under the presumably highly oxidative cellular environment resulting from disturbed lignin biosynthesis. GSTs also mediate conjugation of glutathione to xenobiotics or electrophilic natural products, including phenylpropanoids, for sequestration and/or transport (Dean et al., 1995; Dixon et al., 2010). Thus, the widespread upregulation of *GSTs* in the *4cl1* mutants could also be linked to detoxification of excess phenylpropanoids.

Besides its roles in redox balance and detoxification, glutathione as an abundant low-molecular-weight thiol metabolite is intimately associated with sulfur homeostasis (Takahashi et al., 2011). Many sulfur assimilation pathway genes can be induced by sulfur starvation, or upon Cd exposure, which triggers synthesis of glutathione and its oligomeric phytochelatins for metal chelation, resulting in sulfur depletion (Scheerer et al., 2010; Honsel et al., 2012). Interestingly, two genes belonging to the plant-specific *LSU* family were significantly upregulated in the mutant xylem (Fig. 5), hinting at potential sulfur limitation there. Sulfur assimilation also supplies sulfate donors for sulfation of diverse peptides, proteins, and metabolites (Jez et al., 2016). Indeed, we observed increased abundance in the mutants of two unusual sulfate esters, caffeic acid sulfate and ferulic acid sulfate, though with unknown function (Table 2). Taken together, elevated levels of glutathione conjugation, phenolic acid sulfates, and other sulfated compounds might have depleted available pools of reduced sulfur in the *4cl1* xylem, which in turn activated the sulfur assimilation pathway.

CONCLUSIONS

Our data support differences in regulation and perturbation of lignin biosynthesis between *Populus* and

herbaceous species. We identified the juncture between caffeic acid and caffeoyl-CoA as being highly sensitive to *4CL1*-KO, while also key to modulating the compensatory function of 4CL5. Transcriptional, metabolic, and biochemical coordination of the compensatory pathway likely underscores the species-specific lignin perturbation response reported here. The work raises the enticing possibility that such lineage-specific capability might have originated from taxon-dependent developmental plasticity that warrants future investigation.

MATERIALS AND METHODS

Plant Materials

The *4cl1* mutants and Cas9-only vector controls were reported in Zhou et al. (2015). All mutant lines harbor frameshift mutations in the gRNA target site of *4CL1* (GAGGATGaTaAAaTCTGGAGGGG; the protospacer adjacent motif is underlined and sequence polymorphisms with *4CL5* are in lowercase), which have been reconfirmed using leaves from plants that have been vegetatively propagated and maintained in the greenhouse for over 4 years (Bewg et al., 2018; Supplemental Table S1). *4CL5*-KO plants were produced by targeting the homologous site (GAGGATGtTgAAgTCTGGAGGG). The construct was prepared according to Jacobs and Martin (2016), except two oligos tailed with *Medicago truncatula* U6 (AACTCCAGACTTCAACATCCTCAAGCCTACTGGTTCGCTTGA) or scaffold sequence (GAGGATGTTGAAGTCTGGAGTTTTAGAGCTAGAAATAGCAAGTT; underlined) were used in a half (10 μL) reaction containing 0.005 pmol of linearized p201N vector and 0.1 pmol of inserts (U6, scaffold and the two gRNA oligos) using the Gibson Assembly Master Mix (New England Biolabs). *Agrobacterium*-mediated transformation of *P. tremula* × *alba* INRA 717-1B4 was performed according to Leple et al. (1992). Editing patterns were determined by amplicon-sequencing using *4CL1/4CL5* consensus primers (GTTCAGACGTGTGCTCTTCCGATCTAGCACCGGTTGTHCCA and CCTACACGACGCTCTTCCGATCTGAGGAAACTTRGCTCTGAC) tailed with Illumina sequencing primers (underlined) to check for both on-target and off-target cleavage as described in Zhou et al. (2015). Indexed samples were pooled and sequenced as a spike-in on a NextSeq500 (Illumina) at the Georgia Genomics and Bioinformatics Core, University of Georgia, and the data were analyzed by the open-source software AGEseq (Xue and Tsai, 2015). For characterization, primary transformants in 1-gallon pots were grown to ~2 m in height before harvesting. Developing xylem scrapings were collected at 15 to 30 cm from the top and snap-frozen in liquid nitrogen for RNA and metabolite analyses. The rest of the stem was debarked and air-dried for wood chemical and physical analyses (Supplemental Table S1). Vegetatively-propagated plants were used in histological analysis.

Histology

Stem cross sections (100 μm) were prepared from young shoots using a Vibratome (Ted Pella). Sections were stained with 0.05% (w/v) toluidine blue or 2% (w/v) phloroglucinol in acid ethanol (1 M HCl:95% ethanol = 1:1, v/v), and images were acquired using a Zeiss Axioskop-50 microscope equipped with a Leica DFC500 digital camera.

Wood Specific Gravity and Acoustic Velocity

Three ~8-mm longitudinal stem wood sections were obtained from the base of each sample for nine control (three wild-type and six Cas9 lines) and 12 independent mutant lines. Specific gravity (wood density divided by the density of water) was measured by water displacement after the sections were saturated with water (ASTM International Committee, 2017). Acoustic velocity was measured on the samples before water saturation using a time of flight instrument (SoniSys) equipped with two 1-MHz transducers to send and receive the acoustic signal. The specific gravity and acoustic velocity values from the three sections were averaged for each sample, and statistical differences between groups were determined by Student's *t* test.

Wood Chemistry, Saccharification, and NMR Analysis

The wood samples were ground to pass a 40-mesh screen using a Wiley mill, followed by 99 cycles of ethanol extraction using a Soxhlet extraction unit (Buchi) and air-dried. Extractive-free wood meal was used for Klason lignin (Swamy et al., 2015) and crystalline cellulose content determination according to Updegraff (1969). Lignin composition was determined by thioacidolysis (Foster et al., 2010a), matrix polysaccharide composition by trifluoroacetic acid hydrolysis (Foster et al., 2010b), and glycosyl composition by methanolysis followed by trimethylsilylation (Harding et al., 2018). High-throughput saccharification assays were performed using the BESC method with hot water pretreatment at 180°C for 40 min (Selig et al., 2010), as well as the GLBRC methods using hot water, dilute acid (2% [v/v] H_2SO_4), or dilute base (6.25 mM NaOH) pretreatment at 90°C for 3 h (Santoro et al., 2010). NMR analysis using ball-milled whole cell wall residues or enzyme lignin after cellulase digestion was performed as detailed in Kim and Ralph (2010) and Mansfield et al. (2012b). Unless otherwise noted, these analyses were performed for five controls (three wild-type and two vector controls) and five independent *4cl1* mutants (Supplemental Table S1).

Glycome Profiling

Extractive-free wood meals were sequentially extracted with 50 mM ammonium oxalate, 50 mM sodium carbonate, 1 M KOH, 4 M KOH, acid chlorite, and 4 M KOH to obtain cell wall fractions for screening with a panel of plant glycan-directed mAbs (Pattathil et al., 2010). Statistical analysis of mutant effects was performed with the program Limma (Smyth, 2005) after excluding mAbs with hybridization intensities <0.1 in all samples (three wild-type, three vector controls, and six independent *4cl1* mutants; Supplemental Table S1). mAbs that showed significantly different signal intensities between mutant and control samples ($P \leq 0.01$ and fold-change ≥ 1.5) were visualized by heatmaps using R software.

Phenolic Profiling

Developing xylem scrapings were ground to a fine powder under liquid nitrogen, aliquoted, and stored at −80°C. One aliquot per sample was freeze-dried and 10 mg (dry weight) of tissue were extracted with 400 μL chloroform:methanol (1:1, v/v) in an ultrasonic bath with pre-ice–chilled water for 30 min, followed by addition of 200 μL water, vortexing, and centrifugation for phase separation. The aqueous phase was transferred to a new tube, and an aliquot of 100 μL was evaporated to dryness in a Centrivap (Labconco) for shipment to the Vlaams Instituut voor Biotechnologie. The residues were resuspended in 200 μL of cyclohexane:water (1:1, v/v) and 15 μL were injected onto an Acquity ultra performance liquid chromatography equipped with a Synapt Q-TOF (Waters) for chromatographic separation and mass spectrometric detection of phenolic metabolites following the conditions and settings detailed in Saleme et al. (2017). A total of 10 control (three wild-type and seven *Cas9*) and 14 independent *4cl1* samples were analyzed (Supplemental Table S1). Significant differences between the two groups were declared for peaks that had average signal intensities ≥1,000 counts in at least one group, with $P \leq 0.01$ and fold-change ≥ 2. Compound annotation was based on matching *m/z*, retention time, and tandem mass spectroscopy fragmentation (Supplemental Fig. S5) against an in-house library as well as literature data.

RNA-Seq Analysis and Sample-Specific Coexpression Network Construction

RNA was extracted from frozen xylem powder using the Direct-zol RNA Miniprep kit (Zymo) with PureLink Plant RNA Reagent (Life Technologies) for Illumina RNA-Seq library preparation and NextSeq 500 sequencing as described in Harding et al. (2018). Six control (three wild-type and three *Cas9*) and six *4cl1* independent mutant samples (Supplemental Table S1) were sequenced to obtain 8.3 to 12.1 million paired-end 75-bp reads per sample, except vector control *Cas9-39*, for which >97 M reads were obtained, and only 16-million randomly sampled reads were used for data analysis. After preprocessing for quality control, reads were mapped to the variant-substituted *Populus tremula* × *alba* genome v1.1 as detailed in Xue et al. (2015). Genes satisfying the criteria of FPKM ≥ 5 in at least four out of six replicates of at least one group, average FPKM ≥ 10 in at least one group, $Q \leq 0.05$, and fold-change ≥ 1.5 were used for GO enrichment analysis by the software topGO

(Alexa and Rahnenfuhrer, 2010) with Fisher's exact test, and the negative $\log_{10}$-transformed P values were visualized as heatmaps. For coexpression network analysis, relaxed thresholds ($P \leq 0.05$, FPKM ≥ 5) were used to obtain 5,512 genes that differed between control and *4cl1* plants. The average expression values of the 5,512 genes were calculated for the control and *4cl1* mutant groups. We then adapted the approach of Liu et al. (2016) for construction of genotype-specific networks. Briefly, a group of reference samples was assembled from our previous studies unrelated to lignin pathway gene manipulation (Swamy et al., 2015; Xue et al., 2016). Only unstressed xylem samples were included ($n = 35$). Expression values of the 5,512 genes were extracted from the 35 samples, and the averaged expression values of control or *4cl1* mutant samples were added separately to create two datasets ($n = 36$ each) for construction of the control- and mutant-specific networks. For simplicity, we refer to the former containing the control group (wild-type and *Cas9* lines) as the wild-type network. Pairwise Spearman correlation coefficients of both datasets followed a normal distribution (Supplemental Fig. S4) and were used for weighted gene coexpression network analysis using the WGCNA R package (Langfelder and Horvath, 2008) as detailed in Xue et al. (2016), with a soft threshold of 10. The coexpression relationships were assessed by hierarchical clustering using the topological overlap measure and modules were determined with a dynamic tree cutting algorithm (Supplemental Fig. S4). The list of 5,512 genes, their expression differences between control and *4cl1* mutants, and sample-specific network module assignments are provided in Supplemental Dataset S1.

Accession Numbers

The RNA-seq data has been deposited to the National Center for Biotechnology Information Sequence Read Archive under accession No. PRJNA589632.

Supplemental Data

The following supplemental materials are available.

Supplemental Figure S1. Class-I 4CL gene family members in *Populus*.

Supplemental Figure S2. Glycome profiling analysis of all six cell wall fractions.

Supplemental Figure S3. Characterization of *4cl5* KO mutants.

Supplemental Figure S4. Genotype-specific coexpression network analysis.

Supplemental Figure S5. Tandem mass spectroscopy spectra of metabolites listed in Table 2.

Supplemental Table S1. List of mutant and control plant lines used in this study.

Supplemental Dataset S1. List of differentially expressed genes and their network module assignments.

ACKNOWLEDGMENTS

The authors thank Gilles Pilate of The Institut National de la Recherche Agronomique, France for providing poplar clone INRA 717-1B4, Yenfei Wang (University of Georgia) for assistance with transgenic plant production, Eli McKinney (University of Georgia) for greenhouse plant care, Nicholas Rohr and Bob Schmitz (University of Georgia) for Illumina RNA library construction, Jacob Reeves (University of Georgia) for assistance with data processing and Sequence Read Archive submission, the Georgia Genomics and Bioinformatics Core for Illumina NextSeq sequencing, the Complex Carbohydrate Research Center Analytical Services and Training Laboratory for pyMBMS analysis, and Cliff Foster of the Great Lakes Bioenergy Research Center for cell wall analyses.

Received December 20, 2019; accepted February 26, 2020; published March 6, 2020.

LITERATURE CITED

Alexa A, Rahnenfuhrer J (2010) topGO: Enrichment Analysis for Gene Ontology. R package version 2.0. www.bioconductor.org

ASTM International Subcommittee (2017) ASTM D2395-17: Standard test methods for density and specific gravity (relative density) of wood and wood-based materials. In Book of Standards, Vol **Vol 04.10**. ASTM International, West Conshohocken, PA

Barros J, Escamilla-Trevino L, Song L, Rao X, Serrani-Yarce JC, Palacios MD, Engle N, Choudhury FK, Tschaplinski TJ, Venables BJ, et al (2019) 4-Coumarate 3-hydroxylase in the lignin biosynthesis pathway is a cytosolic ascorbate peroxidase. Nat Commun **10:** 1994

Bewg WP, Ci D, Tsai C-J (2018) Genome editing in trees: From multiple repair pathways to long-term stability. Front Plant Sci **9:** 1732

Boerjan W, Ralph J, Baucher M (2003) Lignin biosynthesis. Annu Rev Plant Biol **54:** 519–546

Chanoca A, de Vries L, Boerjan W (2019) Lignin engineering in forest trees. Front Plant Sci **10:** 912

Chen F, Dixon RA (2007) Lignin modification improves fermentable sugar yields for biofuel production. Nat Biotechnol **25:** 759–761

Chen H-C, Song J, Wang JP, Lin Y-C, Ducoste J, Shuford CM, Liu J, Li Q, Shi R, Nepomuceno A, et al (2014a) Systems biology of lignin biosynthesis in *Populus trichocarpa*: Heteromeric 4-coumaric acid:coenzyme A ligase protein complex formation, regulation, and numerical modeling. Plant Cell **26:** 876–893

Chen H-C, Song J, Williams CM, Shuford CM, Liu J, Wang JP, Li Q, Shi R, Gokce E, Ducoste J, et al (2013) Monolignol pathway 4-coumaric acid:coenzyme A ligases in *Populus trichocarpa*: Novel specificity, metabolic regulation, and simulation of coenzyme A ligation fluxes. Plant Physiol **161:** 1501–1516

Chen H-Y, Babst BA, Nyamdari B, Hu H, Sykes R, Davis MF, Harding SA, Tsai C-J (2014b) Ectopic expression of a loblolly pine class II 4-coumarate:CoA ligase alters soluble phenylpropanoid metabolism but not lignin biosynthesis in *Populus*. Plant Cell Physiol **55:** 1669–1678

Coleman HD, Park J-Y, Nair R, Chapple C, Mansfield SD (2008) RNAi-mediated suppression of p-coumaroyl-CoA 3′-hydroxylase in hybrid poplar impacts lignin deposition and soluble secondary metabolism. Proc Natl Acad Sci USA **105:** 4501–4506

Conti E, Izaurralde E (2005) Nonsense-mediated mRNA decay: Molecular insights and mechanistic variations across species. Curr Opin Cell Biol **17:** 316–325

Dean JV, Devarenne TP, Lee IS, Orlofsky LE (1995) Properties of a maize glutathione s-transferase that conjugates coumaric acid and other phenylpropanoids. Plant Physiol **108:** 985–994

Dixon DP, Skipsey M, Edwards R (2010) Roles for glutathione transferases in plant secondary metabolism. Phytochemistry **71:** 338–350

Ehlting J, Büttner D, Wang Q, Douglas CJ, Somssich IE, Kombrink E (1999) Three 4-coumarate:coenzyme A ligases in *Arabidopsis thaliana* represent two evolutionarily divergent classes in angiosperms. Plant J **19:** 9–20

Foster CE, Martin TM, Pauly M (2010a) Comprehensive compositional analysis of plant cell walls (lignocellulosic biomass) part I: Lignin. J Vis Exp **11:** 1745

Foster CE, Martin TM, Pauly M (2010b) Comprehensive compositional analysis of plant cell walls (lignocellulosic biomass) part II: Carbohydrates. J Vis Exp **12:** 1837

Gao W, Li H-Y, Xiao S, Chye M-L (2010) Acyl-CoA-binding protein 2 binds lysophospholipase 2 and lysoPC to promote tolerance to cadmium-induced oxidative stress in transgenic Arabidopsis. Plant J **62:** 989–1003

Gui J, Shen J, Li L (2011) Functional characterization of evolutionarily divergent 4-coumarate:coenzyme a ligases in rice. Plant Physiol **157:** 574–586

Harding SA, Hu H, Nyamdari B, Xue L-J, Naran R, Tsai C-J (2018) Tubulins, rhythms and cell walls in poplar leaves: It's all in the timing. Tree Physiol **38:** 397–408

Harding SA, Leshkevich J, Chiang VL, Tsai CJ (2002) Differential substrate inhibition couples kinetically distinct 4-coumarate:coenzyme a ligases with spatially distinct metabolic roles in quaking aspen. Plant Physiol **128:** 428–438

Hefer CA, Mizrachi E, Myburg AA, Douglas CJ, Mansfield SD (2015) Comparative interrogation of the developing xylem transcriptomes of two wood-forming species: *Populus trichocarpa* and *Eucalyptus grandis*. New Phytol **206:** 1391–1405

Hoffmann L, Besseau S, Geoffroy P, Ritzenthaler C, Meyer D, Lapierre C, Pollet B, Legrand M (2004) Silencing of hydroxycinnamoyl-coenzyme A shikimate/quinate hydroxycinnamoyltransferase affects phenylpropanoid biosynthesis. Plant Cell **16:** 1446–1465

Hoffmann L, Maury S, Martz F, Geoffroy P, Legrand M (2003) Purification, cloning, and properties of an acyltransferase controlling shikimate and quinate ester intermediates in phenylpropanoid metabolism. J Biol Chem **278:** 95–103

Honsel A, Kojima M, Haas R, Frank W, Sakakibara H, Herschbach C, Rennenberg H (2012) Sulphur limitation and early sulphur deficiency responses in poplar: Significance of gene expression, metabolites, and plant hormones. J Exp Bot **63:** 1873–1893

Hu H, Gu X, Xue L-J, Swamy PS, Harding SA, Tsai C-J (2016) Tubulin C-terminal post-translational modifications do not occur in wood forming tissue of *Populus*. Front Plant Sci **7:** 1493

Hu WJ, Harding SA, Lung J, Popko JL, Ralph J, Stokke DD, Tsai CJ, Chiang VL (1999) Repression of lignin biosynthesis promotes cellulose accumulation and growth in transgenic trees. Nat Biotechnol **17:** 808–812

Hu WJ, Kawaoka A, Tsai C-J, Lung J, Osakabe K, Ebinuma H, Chiang VL (1998) Compartmentalized expression of two structurally and functionally distinct 4-coumarate:CoA ligase genes in aspen (*Populus tremuloides*). Proc Natl Acad Sci USA **95:** 5407–5412

Jacobs TB, Martin GB (2016) High-throughput CRISPR vector construction and characterization of DNA modifications by generation of tomato hairy roots. J Vis Exp **2016:** 53843

Jez JM, Ravilious GE, Herrmann J (2016) Structural biology and regulation of the plant sulfation pathway. Chem Biol Interact **259**(Pt A): 31–38

Kajita S, Katayama Y, Omori S (1996) Alterations in the biosynthesis of lignin in transgenic plants with chimeric genes for 4-coumarate:coenzyme A ligase. Plant Cell Physiol **37:** 957–965

Kim H, Padmakshan D, Li Y, Rencoret J, Hatfield RD, Ralph J (2017) Characterization and elimination of undesirable protein residues in plant cell wall materials for enhancing lignin analysis by solution-state nuclear magnetic resonance spectroscopy. Biomacromolecules **18:** 4184–4195

Kim H, Ralph J (2010) Solution-state 2D NMR of ball-milled plant cell wall gels in DMSO-$d_6$pyridine-d_5. Org Biomol Chem **8:** 576–591

Knobloch KH, Hahlbrock K (1975) Isoenzymes of *p*-coumarate:CoA ligase from cell suspension cultures of *Glycine max*. Eur J Biochem **52:** 311–320

Langfelder P, Horvath S (2008) WGCNA: An R package for weighted correlation network analysis. BMC Bioinformatics **9:** 559

Lee D, Meyer K, Chapple C, Douglas CJ (1997) Antisense suppression of 4-coumarate:coenzyme A ligase activity in *Arabidopsis* leads to altered lignin subunit composition. Plant Cell **9:** 1985–1998

Leple JC, Brasileiro ACM, Michel MF, Delmotte F, Jouanin L (1992) Transgenic poplars: Expression of chimeric genes using four different constructs. Plant Cell Rep **11:** 137–141

Li Y, Kim JI, Pysh L, Chapple C (2015) Four isoforms of Arabidopsis 4-coumarate:CoA ligase have overlapping yet distinct roles in phenylpropanoid metabolism. Plant Physiol **169:** 2409–2421

Lin C-Y, Wang JP, Li Q, Chen H-C, Liu J, Loziuk P, Song J, Williams C, Muddiman DC, Sederoff RR, et al (2015) 4-Coumaroyl and caffeoyl shikimic acids inhibit 4-coumaric acid:coenzyme A ligases and modulate metabolic flux for 3-hydroxylation in monolignol biosynthesis of *Populus trichocarpa*. Mol Plant **8:** 176–187

Lin J-S, Huang X-X, Li Q, Cao Y, Bao Y, Meng X-F, Li Y-J, Fu C, Hou B-K (2016) UDP-glycosyltransferase 72B1 catalyzes the glucose conjugation of monolignols and is essential for the normal cell wall lignification in *Arabidopsis thaliana*. Plant J **88:** 26–42

Lindermayr C, Möllers B, Fliegmann J, Uhlmann A, Lottspeich F, Meimberg H, Ebel J (2002) Divergent members of a soybean (*Glycine max* L.) 4-coumarate:coenzyme A ligase gene family. Eur J Biochem **269:** 1304–1315

Liu X, Wang Y, Ji H, Aihara K, Chen L (2016) Personalized characterization of diseases using sample-specific networks. Nucleic Acids Res **44:** e164

Lu F, Karlen SD, Regner M, Kim H, Ralph SA, Sun R-C, Kuroda K-I, Augustin MA, Mawson R, Sabarez H, et al (2015) Naturally p-hydroxybenzoylated lignins in palms. BioEnergy Res **8:** 934–952

Lu S, Li Q, Wei H, Chang M-J, Tunlaya-Anukit S, Kim H, Liu J, Song J, Sun Y-H, Yuan L, et al (2013) Ptr-miR397a is a negative regulator of laccase genes affecting lignin content in *Populus trichocarpa*. Proc Natl Acad Sci USA **110:** 10848–10853

Mansfield SD, Kang K-Y, Chapple C (2012a) Designed for deconstruction—poplar trees altered in cell wall lignification improve the efficacy of bioethanol production. New Phytol **194:** 91–101

Mansfield SD, Kim H, Lu F, Ralph J (2012b) Whole plant cell wall characterization using solution-state 2D NMR. Nat Protoc **7:** 1579–1589

Molina-Rueda JJ, Tsai C-J, Kirby EG (2013) The *Populus* superoxide dismutase gene family and its responses to drought stress in transgenic poplar overexpressing a pine cytosolic glutamine synthetase (GS1a). PLoS One **8:** e56421

Nakashima J, Chen F, Jackson L, Shadle G, Dixon RA (2008) Multi-site genetic modification of monolignol biosynthesis in alfalfa (*Medicago sativa*): Effects on lignin composition in specific cell types. New Phytol **179:** 738–750

Park J-J, Yoo CG, Flanagan A, Pu Y, Debnath S, Ge Y, Ragauskas AJ, Wang Z-Y (2017) Defined tetra-allelic gene disruption of the 4-coumarate:coenzyme A ligase 1 (Pv4CL1) gene by CRISPR/Cas9 in switchgrass results in lignin reduction and improved sugar release. Biotechnol Biofuels **10:** 284

Pattathil S, Avci U, Baldwin D, Swennes AG, McGill JA, Popper Z, Bootten T, Albert A, Davis RH, Chennareddy C, et al (2010) A comprehensive toolkit of plant cell wall glycan-directed monoclonal antibodies. Plant Physiol **153:** 514–525

Pattathil S, Avci U, Miller JS, Hahn MG (2012) Immunological approaches to plant cell wall and biomass characterization: Glycome profiling. Methods Mol Biol **908:** 61–72

Ralph J, Landucci LL (2010) NMR of lignins. In C Heitner, DR Dimmel, and JA Schmidt, eds, Lignin and Lignans: Advances in Chemistry. CRC Press, Boca Raton, FL, pp 137–234

Ralph J, Lundquist K, Brunow G, Lu F, Kim H, Schatz PF, Marita JM, Hatfield RD, Ralph SA, Christensen JH, et al (2004) Lignins: Natural polymers from oxidative coupling of 4-hydroxyphenyl-propanoids. Phytochem Rev **3:** 29–60

Ranocha P, Chabannes M, Chamayou S, Danoun S, Jauneau A, Boudet AM, Goffner D (2002) Laccase down-regulation causes alterations in phenolic metabolism and cell wall structure in poplar. Plant Physiol **129:** 145–155

Rey P, Tarrago L (2018) Physiological roles of plant methionine sulfoxide reductases in redox homeostasis and signaling. Antioxidants **7:** 114

Rouhier N, Lemaire SD, Jacquot J-P (2008) The role of glutathione in photosynthetic organisms: Emerging functions for glutaredoxins and glutathionylation. Annu Rev Plant Biol **59:** 143–166

Ruprecht C, Bartetzko MP, Senf D, Dallabernadina P, Boos I, Andersen MCF, Kotake T, Knox JP, Hahn MG, Clausen MH, et al (2017) A synthetic glycan microarray enables epitope mapping of plant cell wall glycan-directed antibodies. Plant Physiol **175:** 1094–1104

Saballos A, Sattler SE, Sanchez E, Foster TP, Xin Z, Kang C, Pedersen JF, Vermerris W (2012) Brown midrib2 (Bmr2) encodes the major 4-coumarate:coenzyme A ligase involved in lignin biosynthesis in sorghum (*Sorghum bicolor* (L.) Moench). Plant J **70:** 818–830

Saballos A, Vermerris W, Rivera L, Ejeta G (2008) Allelic association, chemical characterization and saccharification properties of brown midrib mutants of sorghum (*Sorghum bicolor* (L.) Moench). BioEnergy Res **1:** 193–204

Saleme MLS, Cesarino I, Vargas L, Kim H, Vanholme R, Goeminne G, van Acker R, Fonseca FCA, Pallidis A, Voorend W, et al (2017) Silencing CAFFEOYL SHIKIMATE ESTERASE affects lignification and improves saccharification in poplar. Plant Physiol **175:** 1040–1057

Santoro N, Cantu SL, Tornqvist C-E, Falbel TG, Bolivar JL, Patterson SE, Pauly M, Walton JD (2010) A high-throughput platform for screening milligram quantities of plant biomass for lignocellulose digestibility. BioEnergy Res **3:** 93–102

Scheerer U, Haensch R, Mendel RR, Kopriva S, Rennenberg H, Herschbach C (2010) Sulphur flux through the sulphate assimilation pathway is differently controlled by adenosine 5′-phosphosulphate reductase under stress and in transgenic poplar plants overexpressing *gamma-ECS, SO,* or *APR*. J Exp Bot **61:** 609–622

Schimleck L, Dahlen J, Apiolaza LA, Downes G, Emms G, Evans R, Moore J, Pâques L, van den Bulcke J, Wang X (2019) Non-destructive evaluation techniques and what they tell us about wood property variation. Forests **10:** 728

Schmidt D, Schuhmacher F, Geissner A, Seeberger PH, Pfrengle F (2015) Automated synthesis of arabinoxylan-oligosaccharides enables characterization of antibodies that recognize plant cell wall glycans. Chemistry **21:** 5709–5713

Schoch G, Goepfert S, Morant M, Hehn A, Meyer D, Ullmann P, Werck-Reichhart D (2001) CYP98A3 from *Arabidopsis thaliana* is a 3′-hydroxylase of phenolic esters, a missing link in the phenylpropanoid pathway. J Biol Chem **276:** 36566–36574

Sederoff RR, MacKay JJ, Ralph J, Hatfield RD (1999) Unexpected variation in lignin. Curr Opin Plant Biol **2:** 145–152

Selig MJ, Tucker MP, Sykes RW, Reichel KL, Brunecky R, Himmel ME, Davis MF, Decker SR (2010) Lignocellulose recalcitrance screening by integrated high-throughput hydrothermal pretreatment and enzymatic saccharification. Ind Biotechnol (New Rochelle NY) **6:** 104–111

Smyth GK (2005) Limma: Linear models for microarray data. In R Gentleman, V Carey, S Dudoit, R Irizarry, and W Huber, eds, Bioinformatics and Computational Biology Solutions using R and Bioconductor. Springer, New York, pp 397–420

Studer MH, DeMartini JD, Davis MF, Sykes RW, Davison B, Keller M, Tuskan GA, Wyman CE (2011) Lignin content in natural *Populus* variants affects sugar release. Proc Natl Acad Sci USA **108:** 6300–6305

Sun L, Varanasi P, Yang F, Loqué D, Simmons BA, Singh S (2012) Rapid determination of syringyl:guaiacyl ratios using FT-Raman spectroscopy. Biotechnol Bioeng **109:** 647–656

Swamy PS, Hu H, Pattathil S, Maloney VJ, Xiao H, Xue L-J, Chung J-D, Johnson VE, Zhu Y, Peter GF, et al (2015) Tubulin perturbation leads to unexpected cell wall modifications and affects stomatal behaviour in *Populus*. J Exp Bot **66:** 6507–6518

Sykes RW, Gjersing EL, Foutz K, Rottmann WH, Kuhn SA, Foster CE, Ziebell A, Turner GB, Decker SR, Hinchee MAW, et al (2015) Down-regulation of p-coumaroyl quinate/shikimate 3′-hydroxylase (C3′H) and cinnamate 4-hydroxylase (C4H) genes in the lignin biosynthetic pathway of *Eucalyptus urophylla* × *E. grandis* leads to improved sugar release. Biotechnol Biofuels **8:** 128

Takahashi H, Kopriva S, Giordano M, Saito K, Hell R (2011) Sulfur assimilation in photosynthetic organisms: molecular functions and regulations of transporters and assimilatory enzymes. Annu Rev Plant Biol **62:** 157–184

Tsai C-J, Harding SA, Tschaplinski TJ, Lindroth RL, Yuan Y (2006) Genome-wide analysis of the structural genes regulating defense phenylpropanoid metabolism in *Populus*. New Phytol **172:** 47–62

Updegraff DM (1969) Semimicro determination of cellulose in biological materials. Anal Biochem **32:** 420–424

van Acker R, Vanholme R, Storme V, Mortimer JC, Dupree P, Boerjan W (2013) Lignin biosynthesis perturbations affect secondary cell wall composition and saccharification yield in *Arabidopsis thaliana*. Biotechnol Biofuels **6:** 46

Vanholme R, de Meester B, Ralph J, Boerjan W (2019) Lignin biosynthesis and its integration into metabolism. Curr Opin Biotechnol **56:** 230–239

Vanholme R, Storme V, Vanholme B, Sundin L, Christensen JH, Goeminne G, Halpin C, Rohde A, Morreel K, Boerjan W (2012) A systems biology view of responses to lignin biosynthesis perturbations in *Arabidopsis*. Plant Cell **24:** 3506–3529

Voelker SL, Lachenbruch B, Meinzer FC, Jourdes M, Ki C, Patten AM, Davin LB, Lewis NG, Tuskan GA, Gunter L, et al (2010) Antisense down-regulation of 4CL expression alters lignification, tree growth, and saccharification potential of field-grown poplar. Plant Physiol **154:** 874–886

Voytas DF, Gao C (2014) Precision genome engineering and agriculture: Opportunities and regulatory challenges. PLoS Biol **12:** e1001877

Wang JP, Matthews ML, Williams CM, Shi R, Yang C, Tunlaya-Anukit S, Chen H-C, Li Q, Liu J, Lin C-Y, et al (2018) Improving wood properties for wood utilization through multi-omics integration in lignin biosynthesis. Nat Commun **9:** 1579

Weng J-K, Chapple C (2010) The origin and evolution of lignin biosynthesis. New Phytol **187:** 273–285

Wilkerson CG, Mansfield SD, Lu F, Withers S, Park J-Y, Karlen SD, Gonzales-Vigil E, Padmakshan D, Unda F, Rencoret J, et al (2014) Monolignol ferulate transferase introduces chemically labile linkages into the lignin backbone. Science **344:** 90–93

Xiong W, Wu Z, Liu Y, Li Y, Su K, Bai Z, Guo S, Hu Z, Zhang Z, Bao Y, et al (2019) Mutation of 4-coumarate: coenzyme A ligase 1 gene affects lignin biosynthesis and increases the cell wall digestibility in maize *brown midrib5* mutants. Biotechnol Biofuels **12:** 82

Xu B, Escamilla-Treviño LL, Sathitsuksanoh N, Shen Z, Shen H, Zhang YH, Dixon RA, Zhao B (2011) Silencing of 4-coumarate:coenzyme A ligase in switchgrass leads to reduced lignin content and improved fermentable sugar yields for biofuel production. New Phytol **192:** 611–625

Xue L-J, Alabady MS, Mohebbi M, Tsai C-J (2015) Exploiting genome variation to improve next-generation sequencing data analysis and genome editing efficiency in *Populus tremula* × *alba* 717-1B4. Tree Genet Genomes **11:** 82

Xue L-J, Frost CJ, Tsai C-J, Harding SA (2016) Drought response transcriptomes are altered in poplar with reduced tonoplast sucrose transporter expression. Sci Rep **6:** 33655

Xue L-J, Tsai C-J (2015) AGEseq: Analysis of genome editing by sequencing. Mol Plant **8:** 1428–1430

Ye Z-H, Zhong R (2015) Molecular control of wood formation in trees. J Exp Bot **66:** 4119–4131

Zhou X, Jacobs TB, Xue L-J, Harding SA, Tsai C-J (2015) Exploiting SNPs for biallelic CRISPR mutations in the outcrossing woody perennial *Populus* reveals 4-coumarate:CoA ligase specificity and redundancy. New Phytol **208:** 298–301